Laserless quantum gates for electric dipoles in thermal motion

Eric R. Hudson and Wesley C. Campbell

Laserless quantum gates for electric dipoles in thermal motion

Eric R. Hudson[1, 2, 3] and Wesley C. Campbell[1, 2, 3]

[1]*Department of Physics and Astronomy, Los Angeles, California 90095, USA*
[2]*UCLA Center for Quantum Science and Engineering,*
University of California Los Angeles, Los Angeles, California 90095, USA
[3]*Challenge Institute for Quantum Computation, University of California Los Angeles, Los Angeles, California 90095, USA*
(Dated: September 20, 2021)

Internal states of polar molecules can be controlled by microwave-frequency electric dipole transitions. If the applied microwave electric field has a spatial gradient, these transitions also affect the motion of these dipolar particles. This capability can be used to engineer phonon-mediated quantum gates between e.g. trapped polar molecular ion qubits without laser illumination and without the need for cooling near the motional ground state. The result is a high-speed quantum processing toolbox for dipoles in thermal motion that combines the precision microwave control of solid-state qubits with the long coherence times of trapped ion qubits.

Trapped atomic ion qubits have demonstrated the highest-fidelity quantum operations of all systems [1–4], yet challenges remain for their integration into large, scalable platforms. These systems typically rely on laser-driven, phonon-mediated quantum gates, which introduce three issues for producing large-scale devices. First, the production, conditioning, and delivery of the requisite laser light is not yet readily available from integrable subsystems. Second, laser-induced spontaneous scattering from qubits during gate operations limits the achievable gate fidelity [5], which sets the number of physical qubits required to achieve a fault-tolerant logical qubit. Third, these phonon-mediated gates typically require cooling the ions to near the ground state of motion, *i.e.* to the Lamb-Dicke regime, where the spatial extent of the motional state is much smaller than the wavelength of the laser. This adds technical complexity and renders the gate fidelity susceptible to corruption by the heating of the motional modes from nearby surfaces [6].

At present, several solutions to these challenges are being pursued. Integrated photonics could provide a scalable means to deliver the requisite lasers [7, 8], if they can be extended to handle the intensity and short wavelengths necessary for atomic ion qubits [9]. Schemes for laserless gates for atomic ion qubits are likewise under development that use magnetic field gradients [10–20] to couple the internal degrees of freedom to ion motion. Last, 'ultrafast' gate schemes have been developed for atomic ion qubits based on state-dependent forces generated by lasers [21, 22] or magnetic field gradients [23], that can in principle operate outside of the Lamb-Dicke limit.

Here, we consider an alternative route to scalable, trapped ion quantum information processing that uses *electric-field gradients* produced by multipole electrodes, including the trap itself, to couple the internal states of polar molecular ions to collective phonon modes of their Coulomb crystal. By using electrode configurations that produce a uniform electric field gradient, the interaction can be made largely independent of the ion motional state, in contrast to laser-driven gates that require the (optical) Lamb-Dicke limit. As such, these electric-field gradient gates (EGGs) comprise a toolbox that provides fast state preparation and measurement (SPAM), as well as single- and two-qubit gate capabilities for ions *in thermal motion.* EGGs therefore have inherent advantages for scaling, as they combine the precision microwave qubit control enjoyed by solid-state qubits with the long coherence time of trapped ion qubits. This interaction may also be used with Rydberg atomic ions [24]. Further, replacing the electric field gradients with magnetic field gradients allows similar control for the magnetic degrees of freedom of the molecule.

For clarity, in what follows we introduce the basic EGGs interaction with polar molecular ions and show how it can be used for all necessary quantum logic operations. The use of other mechanisms to perform quantum logic operations with molecular ions have previously been discussed, including the electromagnetic dipole-dipole interaction [25], the dipole-phonon and resulting effective dipole-dipole interaction [26], laser-driven dipole-phonon coupling and quantum logic spectroscopy [27, 28] and microwave-driven dipole-phonon coupling via an optical gradient [29]. Interestingly, the experimental requirements for EGGs appear to be significantly more forgiving and achievable with current technology.

To illustrate EGGs, we consider a linear ion chain that may contain both atomic and molecular ions of approximately the same mass (for simplicity, we assume they are equal), and primarily consider motion along one radial (x) direction of the chain, see Fig. 1. In a linear Paul trap, harmonic confinement in the radial directions is provided by a time-dependent electric potential of the form $\Phi(\mathbf{r}, t) = V_o \cos(\Omega_{\mathrm{rf}} t) \left(x^2 - y^2\right) / r_o^2$, where V_o is the amplitude of the radio-frequency voltage applied to the trap electrodes at frequency Ω_{rf} and r_o is the trap field radius. This provides a ponderomotive potential leading to ion motion that can be approximated by the Hamiltonian $\mathcal{H}_o/\hbar = \sum_p \omega_p (a_p^\dagger a_p + \frac{1}{2})$, where ω_p is the frequency of normal mode p. The displacement

of ion i from its equilibrium position can be written as a superposition of displacements of the normal modes: $\hat{x}^{(i)} = \sum_p \sqrt{\hbar/(2m\omega_p)} \mathrm{b}_p^{(i)} (a_p + a_p^\dagger)$ [30] where $\mathrm{b}_p^{(i)}$ is the ith component of the normalized eigenvector $\mathbf{b}_p$ for mode p.

Molecular ions in the chain are assumed to be identical polar molecules, each with a pair of opposite-parity states $\left| g^{(i)} \right\rangle$ and $\left| e^{(i)} \right\rangle$ that represent the -1 and $+1$ eigenstates, respectively, of the Pauli operator $\sigma_Z^{(i)}$ for this effective two-level system of molecule i. Further, each molecule will also possess long-lived, magnetic field insensitive auxiliary states $\left| a^{(i)} \right\rangle$ that can be used for shelving and information storage. The molecules are subject to a static magnetic field $B(z)\hat{\mathbf{x}}$ that defines the quantization axis and whose magnitude has a gradient along $\mathbf{z}$ [31]. $\left| g^{(i)} \right\rangle$ and $\left| e^{(i)} \right\rangle$ represent states with the same total angular momentum projection, m_F, along $\mathbf{x}$. As such an implementation renders the qubit sensitive to magnetic fields, it is likely preferable that the gradient is used for individual addressing of qubits and then the magnetic field returned to e.g. a point where the qubit is magnetically insensitive [32]. The qubit states are separated in energy by the noninteracting Hamiltonian $\mathcal{H}_{\mathrm{mol}}^{(i)}/\hbar = (\Delta^{(i)}/2)\sigma_Z^{(i)}$, with the qubit states chosen such that $\Delta^{(i)}$ is in the radio- or microwave-frequency range (i.e. $\Delta^{(i)} \gg \omega_p$, but still low enough that precision control technology is readily available). These states are connected by an electric dipole transition moment according to $d = \langle e | \mathbf{d} | g \rangle \cdot \hat{\mathbf{x}}$. Physically, these states could be any dipole-connected states, such as rotational states or Ω-, l-, or K-doublets, and they define the Hilbert space of the dipole. These states are typically separated in energy by anywhere from a few kHz to many GHz [33] allowing a wide range of choice in technology for driving EGGs operations.

Transitions between the molecular states can be driven by applying a sinusoidal voltage of frequency ω_{m} and amplitude V_{m} to the Paul trap electrodes to produce an electric field that interacts with the dipole according to $\mathcal{H}_{\mathrm{m}} = -\mathbf{d} \cdot \mathbf{E}_{\mathrm{m}}(\mathbf{r})$. If the electrodes are driven in a dipole configuration (Fig. 1(b)), the electric field due to a time-dependent voltage at the position of the ions is $\mathbf{E}_{E1} \cdot \hat{\mathbf{x}} \approx -V_{\mathrm{m}} \cos(\omega_{\mathrm{m}} t + \phi_{\mathrm{m}})/(2r_o)$. Therefore, transitions driven in this manner are described in the interaction picture with respect to $\mathcal{H}_{\mathrm{mol}}^{(i)}$ by

$$\mathcal{H}_{E1}^{(i)}/\hbar = -d\,\hat{\mathbf{x}} \cdot \mathbf{E}_{E1}/\hbar = \frac{\Omega}{2}\left(\sigma_+^{(i)} e^{\imath\delta^{(i)}t} + \text{h.c.} \right) \quad (1)$$

where $\Omega = dV_{\mathrm{m}}/(2r_o\hbar)$, $\delta^{(i)} = \Delta^{(i)} - \omega_{\mathrm{m}}$, $\sigma_+^{(i)}$ is the Pauli raising operator for the $\{\left| e^{(i)} \right\rangle, \left| g^{(i)} \right\rangle\}$ subspace, and h.c denotes the Hermitian conjugate. We have assumed the microwave phase can be taken to be $\phi_{\mathrm{m}} = 0$, and the rotating wave approximation (RWA) has been used to eliminate the counter-rotating terms.

If, on the other hand, the trap electrodes are driven in a quadrupole configuration (Fig. 1(c)), the electric field due to time-dependent voltage at the position of the ions is $\mathbf{E}_{E2} \cdot \hat{\mathbf{x}} = -2V_{\mathrm{m}} x \cos(\omega_{\mathrm{m}} t + \phi_{\mathrm{m}})/r_o^2$. Therefore, transitions driven in this manner are described in the interaction picture with respect to $\mathcal{H}_{\mathrm{mol}}^{(i)}$ by

$$\mathcal{H}_{E2}^{(i)}/\hbar = -d\,\hat{\mathbf{x}} \cdot \mathbf{E}_{E2}/\hbar$$
$$= \frac{2\Omega}{r_o} \sum_p \sqrt{\frac{\hbar}{2m\omega_p}} \mathrm{b}_p^{(i)} (a_p + a_p^\dagger) \left(\sigma_+^{(i)} e^{\imath\delta^{(i)}t} + \text{h.c.} \right)$$
$$+ x_{\mathrm{eq}} \frac{2\Omega}{r_o} \left(\sigma_+^{(i)} e^{\imath\delta^{(i)}t} + \text{h.c.} \right), \quad (2)$$

where the RWA has been used to eliminate terms that oscillate at $\Delta^{(i)} + \omega_{\mathrm{m}}$. Here, x_{eq} is the equilibrium x position of the trapped ion, which may differ from the microwave field null (due to, $e.g.$, stray static electric fields). For $x_{\mathrm{eq}} = 0$, $\mathcal{H}_{E2}^{(i)}$ only drives 'sideband' transitions that couple differing molecular states while creating or destroying a single phonon in a mode p, while 'carrier' transitions which couple differing molecular states without changing the motional state are driven by $\mathcal{H}_{E1}^{(i)}$. If $x_{\mathrm{eq}} \neq 0$, $\mathcal{H}_{E2}^{(i)}$ may also drive carrier transitions. However, the carrier transition strength arising from $\mathcal{H}_{E2}^{(i)}$ is less than that encountered in laser-based gates [2, 34] as long as $x_{\mathrm{eq}} < 1/\Delta k$, where $\hbar\Delta k$ is the momentum imparted by the atomic ion transition. Thus, the effects of $x_{\mathrm{eq}} \neq 0$ can be mitigated with standard techniques for suppressing carrier transitions in trapped atomic-ion gates [35] and we assume $x_{\mathrm{eq}} = 0$ unless specified.

Because $\nabla \cdot \mathbf{E} = 0$, the gradient along $\hat{\mathbf{x}}$ is accompanied by gradients along $\hat{\mathbf{y}}$ and/or $\hat{\mathbf{z}}$. In principle, these gradients can drive transitions that change m_F by ± 1. However, these transitions experience a Zeeman shift of order $\mu_B B$ (μ_B is the Bohr magneton), and we assume B is large enough that their effect can be neglected. Together, $\mathcal{H}_{E1}$ and $\mathcal{H}_{E2}$ provide a complete set of tools for quantum logic with trapped polar molecular ions that, as we show below, does not require ground-state cooling.

For concreteness, we consider EGGs operations in $^{29}\mathrm{Si}^{16}\mathrm{O}^+$ in a trap with a $\omega_1 = 2\pi \cdot 10$ MHz radial center of mass secular frequency and $r_o = 0.1$ mm. This molecular ion, with a dipole moment of $d \approx (4\,\mathrm{D})/\sqrt{3} = 2.3$ D [36], is particularly attractive as $^{28}\mathrm{Si}^{16}\mathrm{O}^+$ has recently been optically pumped into its ground rovibrational state [37]. While the approximately 43 GHz qubit frequency presents engineering challenges, the nuclear spin $I = 1/2$ of $^{29}\mathrm{Si}^{16}\mathrm{O}^+$ provides a convenient field insensitive subspace for storing quantum information [25].

State preparation and measurement. – Preparation and measurement of a molecular ion quantum state can be achieved using EGGs to produce a state-dependent motional excitation that is detected via a co-trapped atomic ion. The dipole-motion coupling is produced by simultaneously applying, in the quadrupole configuration, two microwave tones resonant with the first-order motional
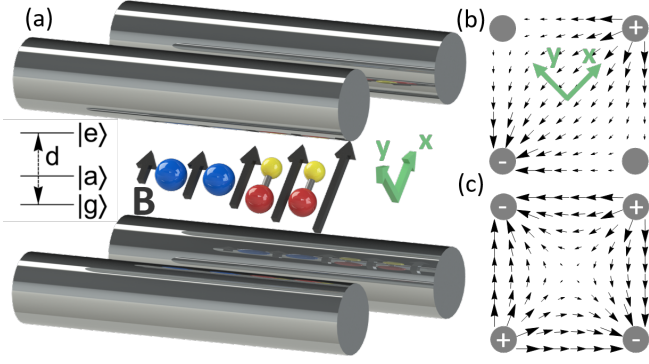
FIG. 1. (a) Schematic of the basic EGGs system. A spatially-varying magnetic field provides individual molecule address-ability. Doppler cooled, co-trapped atomic ions provide sym-pathetic cooling and molecular state-readout capabilities. Ap-plying microwave voltages in a (b) dipole configuration allows single-qubit gates, while a (c) quadrupole configuration pro-vides SPAM and two-qubit gates as described in the text.

FIG. 2. (a) Mean phonon number under application of mi-crowave radiation at $\omega_m^{\pm} = \Delta^{(i)} \pm \omega_1$ with $V_m = 1$ V for an initial thermal state phonon distribution with $T = 1$ mK. Black dots are numerical solutions of Eq. 2 with $x_{eq} = 1$ μm, while the line is the analytical result following from Eq. 4. (b) Two-qubit entangling gate based on Eq. 5 for a $T = 1$ mK thermal state. The black, red, and blue points are the popu-lation in $|g,g\rangle$, $|e,e\rangle$, and $|g,e\rangle + |e,g\rangle$ states as numerically determined from Eq. 2 with $V_m = 1$ V, $\gamma \approx 2\pi \cdot 12$ kHz and $x_{eq} = 1$ μm, while the lines are the same results for $x_{eq} = 0$. The microwave pulses are smoothly turned on and off with a 2 μs time constant.

sidebands of the molecular transition for a motional mode q: $\omega_m^{\pm} = \Delta^{(i)} \pm \omega_q$. Then, in the interaction picture with respect to $\mathcal{H}_o$ and $\mathcal{H}_{mol}^{(i)}$ and neglecting the time-dependent terms, the total Hamiltonian takes the form

$$\mathcal{H}_h^{(i)}/\hbar = 2\Omega\eta_q^{(i)}(a_q + a_q^{\dagger})\sigma_X^{(i)}, \tag{3}$$

where we define $\eta_q^{(i)} \equiv \sqrt{\hbar/(2m\omega_q r_o^2)}b_q^{(i)}$. This interac-tion leads to the time evolution operator

$$U_h^{(i)} = \left|-X^{(i)}\right\rangle\!\left\langle-X^{(i)}\right| D_q\left(2\imath\Omega\eta_q^{(i)}t\right)$$
$$+ \left|+X^{(i)}\right\rangle\!\left\langle+X^{(i)}\right| D_q\left(-2\imath\Omega\eta_q^{(i)}t\right), \tag{4}$$

where $\left|\pm X^{(i)}\right\rangle = \left(\left|g^{(i)}\right\rangle \pm \left|e^{(i)}\right\rangle\right)/\sqrt{2}$ and $D_q(\alpha) \equiv \exp(\alpha a_q^{\dagger} - \alpha^* a_q)$ is the harmonic oscillator displacement operator for mode q. As the average phonon number of a coherent state $|\alpha\rangle$ is $|\alpha|^2$, this interaction adds energy, regardless of the qubit state, to the motional mode in the amount of $\Delta E_q \approx \hbar\omega_q(2\Omega\eta_q^{(i)}t)^2$.

State preparation of molecular ion qubits can then be divided into two regimes: preparation *into* the $\{|g\rangle, |e\rangle\}$ subspace and preparation of pure states *within* the sub-space. For the former, the interaction described by Eq. (4) adds significant energy to the motional mode if the molecule is in the qubit subspace, which is heralded by monitoring a co-trapped atomic ion. A null measure-ment can be followed by molecular population redistri-bution until the molecule is found in the qubit subspace.

If the molecule is in the qubit subspace, state detection is possible by a quantum nondemolition measurement as follows. A molecule-specific, microwave carrier transition in the dipole configuration can transfer molecule i from e.g $|g^{(i)}\rangle$ to $|a^{(i)}\rangle$. A Hadamard gate on the qubit sub-space transfers any population in $|e^{(i)}\rangle$ to $|+X^{(i)}\rangle$. Next,
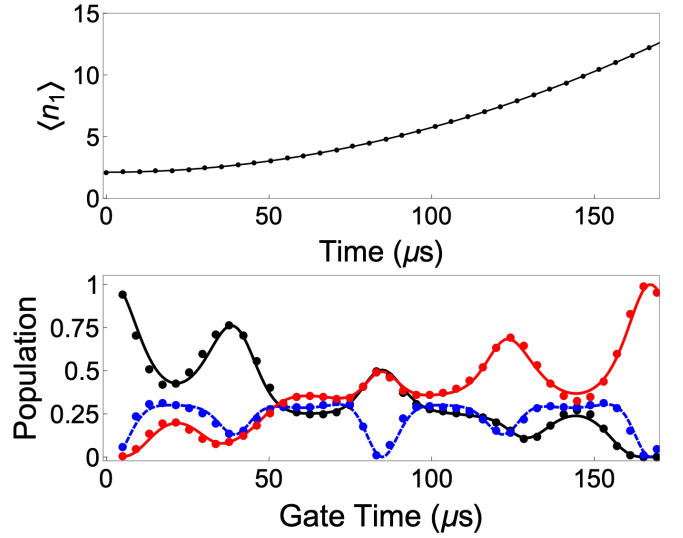
bichromatic microwaves applied in the quadrupole con-figuration add energy to motional mode q (Eq. (3)) if the ion is in $|+X^{(i)}\rangle$. By querying the co-trapped atomic ion (via e.g. the Doppler recooling method [38]), the ion will be found in either $|+X^{(i)}\rangle$ or $|a^{(i)}\rangle$, corresponding to $|e^{(i)}\rangle$ and $|g^{(i)}\rangle$, respectively. Subsequent single-qubit operations can prepare any desired qubit state.

Since $\langle\pm X^{(i)}|\mathbf{d}|\pm X^{(i)}\rangle \cdot \hat{\mathbf{x}} = \pm d$, the state-dependent displacement effected by this bichromatic interaction can be understood as the driving of a time-varying dipole due to the force, $\mathbf{F} = \boldsymbol{\nabla}(\mathbf{d} \cdot \mathbf{E})$, from the time-varying electric field gradient. In contrast to laser-driven mo-tion of atomic ions, where the validity of Eq. (4) quickly breaks down once the displacement becomes compara-ble to the optical wavelength [39, 40], the EGGs force on polar molecular ions remains independent of ion po-sition until the displacement samples non-quadrupolar regions of the electric field. As this typically requires distances comparable to the trap dimensions, large, eas-ily detectable displacements are possible.

For modest experimental parameters ($V_m = 1$ V) the bichromatic interaction adds roughly 10 phonons in 150 μs, shown in Fig. 2(a). If $x_{eq} \neq 0$, carrier transitions become possible and primarily lead to an AC Stark shift. Due to symmetry, if the motional sidebands are driven

with the same amplitude, this Stark shift vanishes and the evolution (black dots) is identical to the previous analytical result (black line).

Single-qubit gates. – Following state preparation, single qubit gates on molecule i are implemented by applying microwave radiation in the dipole configuration at $\omega_\mathrm{m} = \Delta^{(i)}$ and described by $\mathcal{H}_{E1}$. Composite pulse sequences and/or shelving to $\left|a^{(j)}\right\rangle$ can be used to prevent unwanted phase accumulation on nearby molecules.

Interestingly, the electric-field gradient of the trap can also be used to drive carrier quadrupole transitions between, for example, rotational states separated by two rotational quanta. The rate of this transition is roughly $(ea_o^2)\frac{2V}{\hbar r_o^2} \sim 1$ kHz for $V_m = 10$ V, and could be useful for e.g. shelving. Further, additional electrodes providing higher-order multipoles could be used to drive motion on the quadrupole transition.

Molecular two-qubit gates. – As the form of $\mathcal{H}_{E2}$ is similar to the Hamiltonian of an atomic ion qubit subject to a laser in the Lamb-Dicke limit, the two-qubit gates derived from that interaction can be applied to molecular ions via EGGs. As an example, we consider a laserless version of a Mølmer-Sørensen gate [41]. In a chain of trapped molecular ions, two ions can be isolated by shelving all other ions to $|a\rangle$ and the magnetic field gradient adjusted so that the remaining two ions have equal Zeeman shift, i.e. $\Delta^{(1)} = \Delta^{(2)} = \Delta$ (gate operation does not require the ions have equal splittings [42] and is assumed only for simplicity). Next, two microwave tones of equal amplitude at $\omega_\mathrm{m}^\pm = \Delta \pm (\omega_q' + \gamma)$ are applied in a quadrupole arrangement – here ω_q' includes the microwave-field-induced AC Stark shift and γ is the chosen detuning. The time-evolution operator for those two ions in the interaction picture with respect to $\mathcal{H}_o + \mathcal{H}_\mathrm{mol}$ and the microwave-induced Stark shift, after neglecting all time-dependent terms in the Hamiltonian, is

$$U = \exp\left[-\imath \frac{2\Omega^2 \eta_q^{(1)} \eta_q^{(2)}}{\gamma} \sigma_X^{(1)} \sigma_X^{(2)} t\right]. \quad (5)$$

For two molecules initially in the ground qubit state, i.e. $|g, g\rangle$, this interaction produces a Bell state in time $t = \pi\gamma/(2\Omega^2 \eta_q^{(1)} \eta_q^{(2)})$ independent of the phonon states. Taken with the SPAM and single qubit gates described above, EGGs thus provides a universal gate set for trapped molecular ions.

While Eq. (5) is reminiscent of the classic Mølmer-Sørensen (MS) interaction often used to entangle trapped atomic ions through their interaction with a laser, the regime of validity differs for the two cases. Namely, the laser-based MS interaction only takes this form in the Lamb-Dicke limit where the motional state's extent is small enough that electric field amplitude of the laser, with wavevector $\mathbf{k}$, can be approximated as $E_o e^{-\imath \mathbf{k} \cdot \mathbf{x}} \approx E_o(1 - \imath \mathbf{k} \cdot \mathbf{x})$. It is only in this limit, which requires cooling near the ground-state of motion, that the MS interaction is independent of phonon number. However, for EGGs, Eq. (5) remains valid well above the ground state as the relevant length scale for breakdown is the displacement at which the trap field deviates from quadrupolar, i.e. typically a distance of order the trap dimensions. As a result, the EGGs two-qubit gate is, practically speaking, independent of phonon number and can be used on ions in thermal motion.

The independence of the entangling interaction on the motional state is evident in Fig. 2(b), where the evolution of the states $|g, g\rangle$ (black) and $|e, e\rangle$ (red) under the application of two microwave tones at $\omega_\mathrm{m}^\pm = \Delta \pm (\omega_1' + \gamma)$ is shown. Here, the evolution is found numerically from the full Hamiltonian in Eq. 2 for $x_\mathrm{eq} = 0$ (line) and $x_\mathrm{eq} = 1$ μm (dots) with the ions initialized in a thermal state at $T = 1$ mK. Unlike the result in Eq. 5, this calculation is performed in the near-detuned limit with $V_m = 1$ V and $\gamma \approx 2\pi \cdot 12$ kHz, where a faster gate is realized by allowing population to appear in $|ge\rangle$ and $|eg\rangle$ [43]. For all presented calculations, we do not include decoherence sources due to the environment such as state-changing collisions and blackbody redistribution. Given these sources of decoherence are relatively unstudied and likely worse for molecular qubits than atomic qubits (due to the richer internal structure of the former), the experiments proposed here may require operation in a cryogenic environment.

Ultrafast gates. – EGGs also provide the ability to perform entangling operations similar to the so-called "ultrafast" quantum gates that were developed for atomic ion systems [21, 22]. However, because the mechanical effect of EGGs derives from a dipole interacting with a classical, continuous electric field gradient, as opposed to discrete photon recoils so far used in the atomic ion case, its magnitude and direction are simpler to control. If the microwave gradient is applied on resonance for a time that is shorter than $2\pi/\omega_p$ for all p but long compared to $\mu_B B$ and $2\pi/\Delta$, then the evolution of the trapped molecular ions during that time is given solely by $\mathcal{H}_{E2}$ (Eq. (2)). For two molecular ions, such a microwave pulse leads to time evolution given by:

$$\begin{aligned} U_p = \quad &|{-X}\,{-X}\rangle\langle{-X}\,{-X}|\, D_1(2\imath \Delta p_1) \\ &+ |{-X}\,{+X}\rangle\langle{-X}\,{+X}|\, D_2(2\imath \Delta p_2) \\ &+ |{+X}\,{-X}\rangle\langle{+X}\,{-X}|\, D_2(-2\imath \Delta p_2) \\ &+ |{+X}\,{+X}\rangle\langle{+X}\,{+X}|\, D_1(-2\imath \Delta p_1), \quad (6) \end{aligned}$$

where $\Delta p_p = \Omega \eta_p t$ with $\eta_p = |\eta_p^{(i)}|$.

The effect of N such microwave pulses, interspersed with free evolution for time t_ℓ and described by $U_o = \prod_p \exp\left(-\imath \omega_p a_p^\dagger a_p t_\ell\right)$, on an arbitrary coherent state $|\alpha\rangle_p$ can be found by repeated evolution according to $U_o D_p(\pm 2\imath \Delta p_{p,j})$ [21], where $\Delta p_{p,j}$ is the momentum displacement of pulse j applied at time $T_j = \sum_{\ell=1}^{j-1} t_\ell$. If the pulse sequence is constructed such that
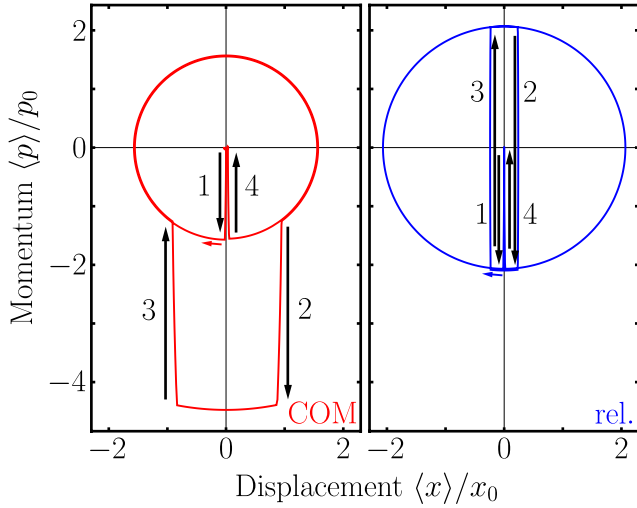
FIG. 3. The phase space trajectory for two ions in the states $|+X+X\rangle$ (red) and $|+X-X\rangle$ (blue). $x_0 \equiv \sqrt{\hbar/2m\omega_p}$ and $p_0 \equiv \sqrt{\hbar m\omega_p/2}$ are the position and momentum space widths of the ground state wavefunctions in the center of mass (red) and relative (blue) modes. Arrows indicate the action of the four pulses.

$\sum_{j=1}^{N} \Delta p_{p,j} e^{\imath \omega_p T_j} = 0$ for $p = 1, 2$, the effect is to return the molecules to their original motional state with an accumulated state-dependent phase. In this case, the time-evolution operator becomes

$$U_N = e^{\imath \Phi \sigma_X^{(1)} \sigma_X^{(2)}} \prod_p e^{-\imath \omega_p a_p^\dagger a_p T_j} \tag{7}$$

$$\Phi = 2 \sum_{j=2}^{N} \sum_{k=1}^{j-1} \Delta p_{1,j} \Delta p_{1,k} \left(\sin\left(\omega_1 (T_j - T_k)\right) \right.$$
$$\left. - \sqrt[4]{3} \sin\left(\frac{\omega_1}{\sqrt{3}}(T_j - T_k)\right) \right) \tag{8}$$

and if $\Phi = \pi/4$, this accomplishes a controlled phase gate.

This result is identical to that in Ref. [21, 22], though in the X basis instead of Z, and the pulse sequences presented by those authors are applicable for ultrafast EGGs. Figure 3 shows trajectories under the pulse sequence defined as 'protocol 1' in Ref. [21]. Here, for population in the $|\pm X \pm X\rangle$ subspace, the center-of-mass mode is excited, while if the molecules are in the $|\pm X \mp X\rangle$ subspace, the relative mode is excited. These trajectories are insensitive to $x_{\mathrm{eq}} \neq 0$ as the $|\pm X\rangle$ are all eigenstates of the carrier interaction, which manifests itself only as a state-dependent phase. However, Φ is also insensitive to the value of x_{eq} since the accumulated phase due to the carrier interaction from the first two pulses is removed by the second two pulses. The ultrafast gate is therefore robust to static offset fields. The build-ing blocks that make this gate, as well as the MS interaction described above, can also be extended to include operations with co-trapped atomic ions whose motion is driven by lasers, allowing for hybrid applications requiring atom-molecule entanglement. Further, recent work on these schemes are continuing to improve the speed and robustness of the laser-driven atomic operations, which will ease their compatibility with EGGs operations in a hybrid scenario [44].

In summary, by using engineered electric-field gradients to drive transitions between electric-dipole-connected polar molecule internal and external states it is possible to construct a set of quantum logic gates that are largely independent of the motional state of the molecule. Since the molecular qubits are controlled by microwave frequency voltages, this technique combines many of the desirable features of solid-state qubits with the long coherence times of trapped ion qubits. The use of electric dipole transitions may provide several advantages over schemes using magnetic dipole transitions [10–16], including a much stronger coupling to far-field electromagnetic radiation and the replacement of the need for high current (in vacuo) with a need for high voltage for local control fields. The calculations presented here have used modest experimental parameters that are routinely surpassed in many laboratories. Significant improvements of these parameters and the concomitant improvements in gate times and fidelities can be expected with additional techniques like superconducting microwave stripline resonators [45]. As a result, and in combination with the techniques of Ref. [25, 26] and the possibility for robust encoding of qubits in rigid rotors [46], polar molecular ions are a promising system for constructing a large, scalable platform for quantum information science.

[1] J. E. Christensen et al., npj Quantum Inf. **6**, 35 (2020).
[2] C. Ballance et al., Phys. Rev. Lett. **117**, 060504 (2016).
[3] T. P. Harty, D. T. C. Allcock, C. J. Ballance, L. Guidoni, H. A. Janacek, N. M. Linke, D. N. Stacey, and D. M. Lucas, Phys. Rev. Lett. **113**, 220501 (2014).
[4] J. P. Gaebler, T. R. Tan, Y. Lin, Y. Wan, R. Bowler, A. C. Keith, S. Glancy, K. Coakley, E. Knill, D. Leibfried, and D. J. Wineland, Phys. Rev. Lett. **117**, 060505 (2016).
[5] R. Ozeri, W. Itano, R. Blakestad, J. Britton, J. Chiaverini, J. Jost, C. Langer, D. Leibfried, R. Reichle, S. Seidelin, J. Wesenberg, and D. Wineland, Phys. Rev. A **75**, 042329 (2007).
[6] J. Sedlacek et al., Phys. Rev. A **97**, 020302(R) (2018).
[7] R. J. Niffenegger, J. Stuart, C. Sorace-Agaskar, D. Kharas, S. Bramhavar, C. D. Bruzewicz, W. Loh, R. T. Maxson, R. McConnell, D. Reens, G. N. West, J. M. Sage, and J. Chiaverini, Nature **586**, 538 (2020).
[8] K. K. Mehta, C. Zhang, M. Malinowski, T.-L.

Nguyen, M. Stadler, and J. P. Home, arXiv preprint arXiv:2002.02258 (2020).

[9] K. K. Mehta, C. D. Bruzewicz, R. McConnell, R. J. Ram, J. M. Sage, and J. Chiaverini, Nature Nanotechnology **11**, 1066 (2016).

[10] F. Mintert and C. Wunderlich, Phys. Rev. Lett. **87**, 257904 (2001).

[11] M. Johanning, A. Braun, N. Timoney, V. Elman, W. Neuhauser, and C. Wunderlich, Phys. Rev. Lett. **102**, 073004 (2009).

[12] A. Khromova, C. Piltz, B. Scharfenberger, T. F. Gloger, M. Johanning, A. F. Varón, and C. Wunderlich, Phys. Rev. Lett. **108**, 220502 (2012).

[13] C. Ospelkaus, C. E. Langer, J. M. Amini, K. R. Brown, D. Leibfried, and D. J. Wineland, Phys. Rev. Lett. **101**, 090502 (2008).

[14] C. Ospelkaus, U. Warring, Y. Colombe, K. R. Brown, J. M. Amini, D. Leibfried, and D. J. Wineland, Nature **476**, 181 (2011).

[15] K. R. Brown, A. C. Wilson, Y. Colombe, C. Ospelkaus, A. M. Meier, E. Knill, D. Leibfried, and D. J. Wineland, Phys. Rev. A **84**, 030303 (2011).

[16] N. Timoney, I. Baumgart, M. Johanning, A. F. Varón, M. B. Plenio, A. Retzker, and C. Wunderlich, Nature **476**, 185 (2011).

[17] T. Harty et al., Phys. Rev. Lett. **117**, 140501 (2016).

[18] S. Weidt et al., Phys. Rev. Lett. **117**, 220501 (2016).

[19] arXiv:2102.12533 (2021).

[20] Phys. Rev. Lett. **123**, 260503 (2019).

[21] J. García-Ripoll, P. Zoller, and C. Cirac, Phys. Rev. Lett. **91**, 157901 (2003).

[22] L. Duan, Phys. Rev. Lett. **93**, 100502 (2004).

[23] J. Mur-Petit, J. J. García-Ripoll, J. Pérez-Ríos, J. Campos-Martínez, M. I. Hernández, and S. Willitsch, Phys. Rev. A **85**, 022308 (2012).

[24] C. Zhang, F. Pokorny, W. Li, G. Higgins, A. Pöschl, I. Lesanovsky, and M. Hennrich, Nature **580**, 345 (2020).

[25] E. R. Hudson and W. C. Campbell, Phys. Rev. A **98**, 040302(R) (2018).

[26] W. C. Campbell and E. R. Hudson, Phys. Rev. Lett. **125**, 120501 (2020).

[27] F. Wolf et al., Nature **530**, 457 (2016).

[28] C.-W. Chou et al., Nature **545**, 203 (2017).

[29] M. Shi et al., New J. Phys. **15**, 113019 (2013).

[30] D. F. V. James, Appl. Phys. B **66**, 181 (1998).

[31] S. Wang, J. Labaziewicz, Y. Ge, R. Shewmon, and I. Chuang, Appl. Phys. Lett. **94**, 094103 (2009).

[32] C. Langer et al., Phys. Rev. Lett. **95**, 060502 (2005).

[33] J. M. Brown and A. Carrington, *Rotational Spectroscopy of Diatomic Molecules*, Cambridge Molecular Science (Cambridge University Press, 2003).

[34] P. Schindler et al., New J. Phys. **15**, 123012 (2013).

[35] G. Kirchmair et al., New J. Phys. **11**, 023002 (2009).

[36] Z.-L. Cai and J. Franois, Chemical Physics **234**, 59 (1998).

[37] P. R. Stollenwerk, I. O. Antonov, S. Venkataramanababu, Y.-W. Lin, and B. C. Odom, Phys. Rev. Lett. **125**, 113201 (2020).

[38] T. Sikorsky et al., Phys. Rev. A **96**, 012519 (2017).

[39] M. J. McDonnell, J. P. Home, D. M. Lucas, G. Imreh, B. C. Keitch, D. J. Szwer, N. R. Thomas, S. C. Webster, D. N. Stacey, and A. M. Steane, Phys. Rev. Lett. **98**, 063603 (2007).

[40] U. Poschinger, A. Walther, K. Singer, and F. Schmidt-Kaler, Phys. Rev. Lett. **105**, 263602 (2010).

[41] K. Mølmer and A. Sørensen, Phys. Rev. Lett. **82**, 1835 (1999).

[42] I. Inlek, C. Crocker, M. Licthman, K. Sosnova, and C. Monroe, Phys. Rev. Lett. **118**, 250502 (2017).

[43] A. Sørensen and K. Mølmer, Phys. Rev. Ad **62**, 022311 (2000).

[44] V. Schäfer et al., Nature **555**, 75 (2018).

[45] D. Schuster et al., Phys. Rev. A **83**, 012311 (2011).

[46] V. Albert, J. Covey, and J. Preskill, Phys. Rev. X **10**, 031050 (2020).